Descriptive Image-Text Matching with Graded Contextual Similarity

Jinhyun Jang, Jiyoung Lee*, Kwanghoon Sohn*

***Abstract*—Image-text matching aims to build correspondences between visual and textual data by learning their pairwise similarities. Most existing approaches have adopted sparse binary supervision, indicating whether a pair of images and sentences matches or not. However, such sparse supervision covers a limited subset of image-text relationships, neglecting their inherent many-to-many correspondences—an image can be described in numerous texts at different descriptive levels. Moreover, existing approaches overlook the implicit connections from general to specific descriptions, which form the underlying rationale for the many-to-many relationships between vision and language. In this work, we propose descriptive image-text matching, called DITM, to learn the graded contextual similarity between image and text by exploring the descriptive flexibility of language. We formulate the descriptiveness score of each sentence with cumulative term frequency-inverse document frequency (TF-IDF) to balance the pairwise similarity according to the keywords in the sentence. Our method leverages sentence descriptiveness to learn robust image-text matching in two key ways: (1) to refine the false negative labeling, dynamically relaxing the connectivity between positive and negative pairs, and (2) to build more precise matching, aligning a set of relevant sentences in a generic-to-specific order. By moving beyond rigid binary supervision, DITM enhances the discovery of both optimal matches and potential positive pairs. Extensive experiments on MS-COCO, Flickr30K, and CxC datasets demonstrate the effectiveness of our method in representing complex image-text relationships compared to state-of-the-art approaches. In addition, DITM enhances the hierarchical reasoning ability of the model, supported by the extensive analysis on HierarCaps benchmark.**

***Index Terms*—Image-text matching, cross-modal retrieval, vision-language model, metric learning.**

I. Introduction

Image-text matching (ITM) [1]–[4], *i.e.*, retrieval of the most relevant image-text pair from a database using either an image or text as a query, has emerged as a fundamental research topic in the multimodal community with wide-ranging applications in search systems. The interest is to learn pairwise similarities of images and texts in a shared embedding space [5], [6]. However, given that the real-world vision and language data inherently include many-to-many correspondences [7], such one-to-one pairwise learning has still remained challenging.

Most ITM benchmarks [8], [9] provide sparse correspondences over visual and textual data. For example, MS-COCO [8] defines a positive match for an image to limited five sentences. Since images and corresponding texts are collected on a large scale, the database contains noisy pairs where the label is negative but still shares semantic relevance (*i.e.*, false negatives). However, standard objectives for ITM, such as triplet loss [1], [5], [10]–[12], solely rely on this sparse binary supervision, enforcing potential correct matches to be penalized. While they present high accuracy on the positive pairs, they often fail to learn the implicit relationships from the false negative pairs, resulting in a twisted embedding space, as shown in Fig. 2-(a) [4], [13].

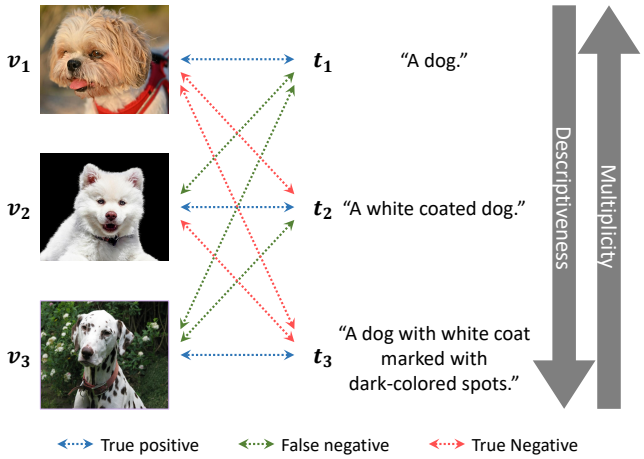

Fig. 1: An example of the ambiguous many-to-many problem in ITM. Only a sparse set of image-text pairs (v_i, t_i) are labeled as positive in ITM benchmarks, leading to the other pairs $(v_i, t_j)_{i \neq j}$ being treated as negatives. However, each sample shares common semantics across diverse samples, regardless of the ground-truth matches.

The straightforward solution is to increase annotations by identifying additional correspondence within the database [3], [4], [14]. They exploit text similarities for adaptive discrimination by measuring similarities between existing paired texts and query text with pretrained language models [14] or captioning metric (*e.g.*, CIDEr [15]) [3], [4]. However, text similarities often lead to improper correspondences. Since the text has an abstract nature than the image, it is not accurate to represent text similarity as the image-text relevance score.

To address this issue, probabilistic approaches [13], [16]–[18] have pointed out the ambiguity problem of deterministic approaches; diverse contexts of an instance are insufficiently represented by a single embedding vector. These approaches encode each instance as a distribution function, allowing many-to-many correspondences to be represented via distributional overlap. While this strategy captures inherent complexity of image-text relationships through predictive uncertainty,

Jinhyun Jang and Kwanghoon Sohn are with the School of Electrical and Electronic Engineering, Yonsei University, Seoul, Korea.
E-mail: {jr000192, khsohn}@yonsei.ac.kr.
Jiyoung Lee is with Ewha Womans University, Seoul, Korea.
E-mail: lee.jiyoung@ewha.ac.kr.
(Corresponding authors: Jiyoung Lee and Kwanghoon Sohn)

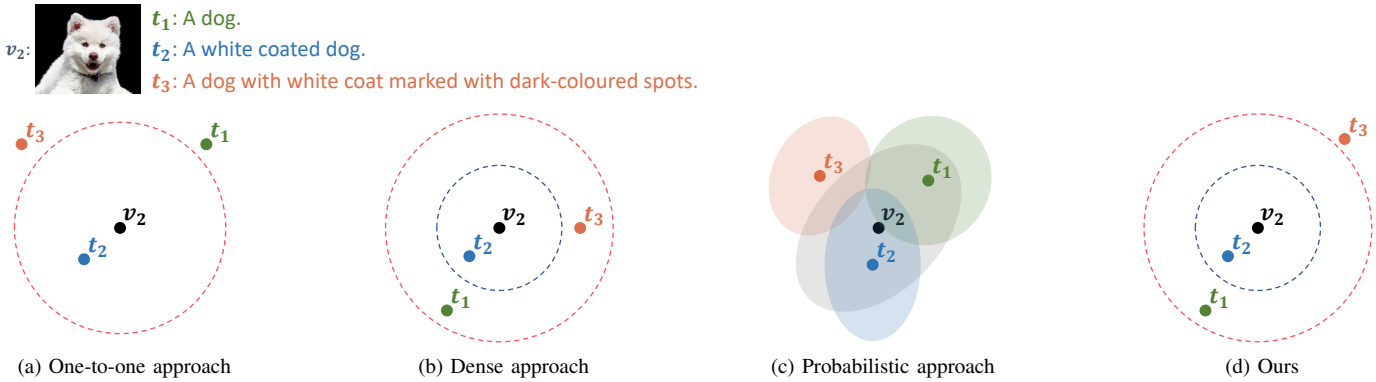

(a) One-to-one approach (b) Dense approach (c) Probabilistic approach (d) Ours

Fig. 2: Comparisons of different objective functions. Given image-text pairs in Fig. 1, we illustrate how each sample is mapped to a common embedding space. The top visualization summarizes the conceptual space, while (a)–(d) show different approaches. The dotted line indicates graded contextual similarity between an image v_2 and other sentences (blue: relevant, red: irrelevant). (a) Standard approaches ignore possible correspondences in false negative pairs; t_1 is learned to be separated from v_2. (b) Dense labeling approaches define contextual similarities of (v_2, t_1) and (v_2, t_3) based on text similarities of (t_2, t_1) and (t_2, t_3), respectively. (c) Probabilistic approaches approximate image-text correspondences by sampling from the learned distribution. (d) Ours alleviates binary labeling based on sentence descriptiveness, capturing graded contextual similarity.

it often results in decreased accuracy due to approximation errors and redundant learned representations [19], [20].

In this work, we build upon the observation that textual descriptions of a visual scene can vary greatly, as language inherently provides multiple levels of abstraction for the same visual content. Given images of a dog with different breeds as in Fig. 1, all images can visualize a general description "a dog" (t_1), while only a Dalmatian image (v_3) can portray a description with instance-specific cues, such as "white coat" and "dark-colored spots" (t_3). This descriptive flexibility suggests that a common representation should reflect graded contextual similarity between images and texts to better capture complex many-to-many correspondences. In addition, this graded approach effectively reduces the impact of false negatives in a mini-batch training scheme, where possible positive pairs are mistakenly treated as negatives, by assigning differential penalties rather than relying on rigid binary supervision.

In this paper, we propose a novel descriptive image-text matching (DITM) to learn many-to-many cross-modal relationships by exploiting the descriptive level of each sentence. Unlike previous methods that newly define the correspondence for every image-sentence pair [3], [4], [14] or rely on predictive uncertainty [13], [16]–[18], ours freely alleviates the lack of binary labels on ITM benchmarks by introducing a hierarchical relative distance to cross-modal representations. The descriptiveness score of each sentence (*i.e.*, information level) is formulated as a cumulative term frequency-inverse document frequency (TF-IDF) [21], [22] such that a larger weight is assigned to the sentence with more instance-specific description. The descriptiveness score is incorporated into ITM objectives for two key aspects. First, we propose an adaptive triplet loss to avoid incorrect discrimination of relevant samples. Less descriptive sentences provide weaker constraints, allowing possible correspondences in false negative pairs to be preserved. This ensures that ambiguous but potentially correct matches are not overly penalized. Secondly, we introduce a generic-to-specific ordering loss to align a set of relevant descriptions of the same image in a generic-to-specific order. Sentences describing the same image are aligned in a hierarchy, from broad to more detailed ones. To achieve this, we adjust the relative distances between image-sentence pairs in the embedding space such that pairs with more descriptive sentences are positioned more distinctly.

In the experiments, we compare our method with the previous ITM objective functions [1]–[4], [13], [16] and demonstrate the effectiveness of our DITM, achieving state-of-the-art performance on four ITM benchmarks: MS-COCO [8], Flick30K [9], Crisscrossed Captions [23], and HierarCaps [24] datasets. Furthermore, extensive ablation studies on the HierarCaps dataset indicate that our learned image-text relationships align well with our initial intuition. Notably, 1) the sentence descriptiveness we define accurately reflects the sentence hierarchy in the HierarCaps dataset, and 2) the distances of the learned image-text representations follow a generic-to-specific ordering consistent with the visual-semantic hierarchy.

II. Related Work

A. Image-text matching

The goal of ITM is to learn the similarity between images and texts while bridging the heterogeneous gap between vision and language. One promising direction is to compare every local component from each modality. Specifically, fusion-based approaches [25]–[29] predict the relevance of an image-text pair by extensively aggregating local region-word similarity scores through cross-attention mechanism. Despite their strong performance, they require every possible pair of images and texts to be jointly fed into the cross-attention module, resulting in high computational overhead. In contrast, dual-encoder methods have been proposed to learn separate vision and language encoders that embed each modality into a shared embedding space. The relevance of each pair is computed by a nearest neighbor search on embedding vectors, making them compatible with large-scale indexing. While these approaches have resolved the scalability issue, the inherent many-to-many correspondences across image-text pairs remain problematic. To address this, a single embedding vector has been extended

v_1: t_1^1: A man sitting on a bench next to his **dog**. (0.36)
t_2^1: An **old** man is **reading** a **book** on a bench with a **dog**. (0.40)
t_3^1: A man reading a **newspaper** while sitting on a **park** bench with his **dog**. (0.43)

v_2: t_1^2: A man that is sitting down on a bench. (0.32)
t_2^2: The man sits on a bench **reading** with a cup of **coffee**. (0.39)
t_3^2: A man with a **drink**, a **book** and a **bag** sits on a bench by an **urn** with a **shrub, brick** and **facade** of a **building**. (0.68)

Fig. 3: An example of the sentence descriptiveness obtained with the cumulative TF-IDF scores. Each image and sentence is marked with the same color if labeled as positive in ITM benchmarks. The numbers are rounded to two decimal places for clear illustration. The most general description t_1^2 has the smallest descriptiveness, and the value increases as the description includes more instance-specific information (*e.g.*, drink, dog).

to a set of heterogeneous embedding vectors [19], [20] via a set prediction module (e.g., self-attention, slot attention [30]) to model diverse contexts of a single instance. Similarly, regional embeddings [31], [32] and probabilistic representations [13], [16]–[18] have been introduced to represent a range of possible interpretations of an instance. However, the embedding sets often encode redundant semantics, leading to degraded performance and increased computational complexity.

B. Metric learning

The typical objective of ITM is to enlarge similarity of positive pairs and reduce similarity of negative pairs [5], [10], [11]. To enable fine-grained distinctions between confusing instances, hardest negative mining strategies [1], [6], [12] enforce stronger penalties on the most challenging negative samples, *i.e.*, those with high similarity to queries. However, they often treat semantically relevant pairs as hardest negatives, intensifying the problem of sparse correspondences between images and texts. To address this, some works rather focus on easy samples [33], [34] that are clearly distinct from the query. While they improve training stability by reducing the impact of ambiguous data, the model performs poorly in real-world scenarios with harder samples. Instead of relying on model predictions to mine important samples, other works [3], [4], [14] densely define image-text relationships via text-text similarities. However, they heavily rely on the quality of similarity measures (*e.g.*, language models [14], captioning metric [3], [4]), and are insufficient to represent image-text relevance, since language descriptions are abstractions of visual information. While sharing a similar spirit with their works, we explore the sentence descriptiveness scores to alleviate the sparse correspondences between vision and language.

Inspired by advances in visual metric learning, our work focuses on constructing a continuous embedding space tailored for cross-modal alignment. Kim et al. [35] formulated the relevance of two images based on their label distances to learn a continuous embedding space. Similarly, class hierarchical trees [36], [37] and word ontology [38], [39] have been explored as a continuous label. We incorporate a common goal of learning continuous embedding spaces into ITM, and explore the information level in descriptions to alleviate the limitations of sparse binary supervision of ITM benchmarks [8], [9].

III. Method

A. Motivation and overview

Given image-text pairs, the goal of ITM is to align cross-modal embeddings with pairwise similarity learning. Existing vision-language datasets consist of texts describing individual images but do not account for relationships between different images or texts (*i.e.*, sparse annotation). As a result, when the dataset size increases, naturally related images and texts become scattered throughout the dataset—yet they are still treated as entirely negative pairs, leading to incorrect associations. Although previous works have defined the relevance of each pair based on sparse binary supervision [1], [5], [10]–[12], predictive uncertainty [13], [16]–[18], and continuous text similarities [3], [4], [14], these approaches passed over the descriptive flexibility of language expression, which serves as the underlying rationale for the many-to-many relationships between vision and language. For example, general descriptions (*e.g.*, a photo, a painting) share common semantics with a lot of specific descriptions and images. In other words, a sentence describes more or fewer images depending on how much detail it conveys [40]–[43]. Thus, the descriptive level of sentences should be considered in the matching objective to learn a robust embedding space.

To this end, we present a novel image-text matching strategy, DITM, that exploits the descriptive levels of sentences to handle the many-to-many relationships between vision and language. To measure hierarchical contextual similarity of image-text pairs, we define the sentence descriptiveness score as the cumulative term frequency-inverse document frequency (TF-IDF) [21], [22] of the words in the given sentence without further learnable modules or increasing training costs (Sec. III-B). We incorporate the descriptiveness score in relaxing the false-negative samples (Sec. III-C), and aligning multiple relevant sentences of images in generic-to-specific order to mimic the humans' hierarchical understanding [24] (Sec. III-D).

B. Sentence descriptiveness score

Vision-language datasets inherently include missed image-text pairs in their heuristic annotation processes. Recently, web-crawled datasets [44], [45] have been grown in scale, and provide weak supervision for a data sample (*i.e.*, image-text acquired simultaneously is provided as a pair). However, building new image-text pairs [23], [24] requires enormous cost and time, which is limited in practice. Our DITM cast

this problem as relaxing the contrastive loss with the penalized term. We motivate the idea [24], [43], [46] that simple sentences can describe many images, while sentences with many detailed descriptions can describe few images. For its concrete realization in a simple yet low-cost way, we formulate a descriptiveness score for each sentence using a cumulative term frequency-inverse document frequency (TF-IDF), which quantifies the importance of each word in the sentence based on the statistics of the whole dataset. Motivated by [21], [22], we assume that sentences containing more uncommon words (*i.e.*, words that do not overlap with other sentences) provide more instance-specific information. Given a set of the sentences $\mathcal{T} = \{t_1, t_2, \ldots, t_M\}$, the TF-IDF score of a word w in a sentence t is defined as:

$$\text{TF-IDF}(w, t) = \frac{N_w}{N} \log \frac{M}{M_w}, \tag{1}$$

where N_w is the number of word w in the sentence t, N is the total number of words in t, and M_w is the number of sentences that contain the word w in the collection $\mathcal{T}$. We consider the frequency of the word both in the sentence and the whole document (*e.g.*, training dataset). The score is thereby the product of the two measurements: (1) the term frequency, N_w/N, which measures the frequency of the word in the given sentence, and (2) the inverse document frequency, $\log M/M_w$, which measures the inverse frequency of the word in the document. The TF-IDF score semantically regards the word that appears frequently only in certain sentences as important. Consequently, a sentence descriptiveness score $\delta(t)$ is derived as the cumulative TF-IDF scores:

$$\delta(t) = \sum_{w}^{N} \text{TF-IDF}(w, t). \tag{2}$$

We apply min-max normalization for scores in training set to $[0, 1]$ to stabilize the training.

C. Learning to preserve shared semantics of common texts

Previous ITM objectives such as triplet loss [1] overlook the descriptive flexibility of language and enforce a fixed margin across all negative samples, leading to wrong separation from their relevant images. To handle this problem, we introduce an adaptive triplet loss to dynamically discriminate positive and negative pairs and relax penalties for false negatives.

Conventional triplet loss. The hinge-based triplet ranking loss [10], [47] with online hard negative mining [1], which is commonly used in ITM, is formulated as:

$$\begin{aligned}\mathcal{L}_{\text{Trp}} = \sum_{(v,t)} &[\alpha - s(v,t) + s(v,t^-)]_+ \\ &+ [\alpha - s(v,t) + s(v^-,t)]_+,\end{aligned} \tag{3}$$

where $[\cdot]_+$ is the hinge function, α is a margin to control the decision boundary between positive and negative pairs, and $s(\cdot,\cdot)$ represents the cosine similarity between L2-normalized visual and textual embeddings. We denote a positive image-sentence pair in the dataset as (v, t). The online hardest negative samples of image and sentence are denoted as $v^- = \text{argmax}_{v' \neq v} s(v', t)$ and $t^- = \text{argmax}_{t' \neq t} s(v, t')$, respectively.

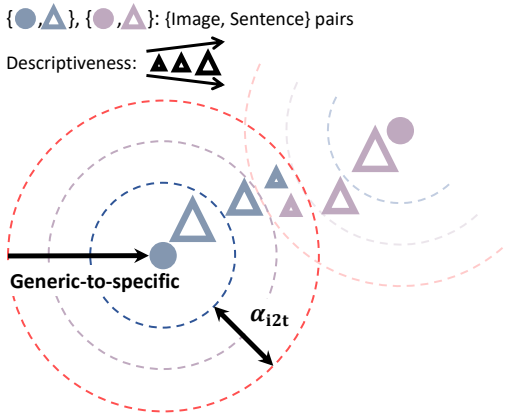

Fig. 4: A conceptual illustration of our framework. We enforce weak constraints on the general descriptions such that its common semantics across other relevant images are preserved. Moreover, the pairwise image-sentence distances are approximated by the sentence descriptiveness, ensuring that the graded contextual similarities reflect the generic-to-specific order.

Based on cosine similarity, these hardest negatives correspond to the image and sentence most similar to (v, t) among the others. The objective penalizes triplets that violate a rank constraint, ensuring the similarity of a positive pair to exceed that of its hardest negative pair by at least the margin α. However, due to the sparse annotations of ITM benchmarks, the objective often misidentifies relevant samples as the hardest negatives, *i.e.*, false negatives. For example, as shown in Fig. 3, given an image v_1 and sentences t_1^1, t_1^2 within the same batch, the potentially positive sample t_1^2 may be incorrectly selected as the hardest negative sample for v_1. In addition, the fixed margin enforces the same separation across all selected triplets, regardless of their varying contextual similarities.

Adaptive triplet loss. To avoid over-penalization on potentially correct matches, we introduce an adaptive triplet loss that dynamically discriminates each pair with respect to the descriptive degree of the paired sentence. Formally, we define an adaptive margin as a sum of sentence descriptiveness scores in the positive and negative pairs being compared, such that:

$$\begin{aligned}\alpha_{\text{i2t}} &= (\delta(t) + \delta(t^-))/\tau, \\ \alpha_{\text{t2i}} &= (\delta(t) + \delta(t))/\tau,\end{aligned} \tag{4}$$

where τ is a scaling factor. Therefore, our adaptive triplet loss is as follows:

$$\begin{aligned}\mathcal{L}_{\text{AdaTrp}} = \sum_{(v,t)} &[\alpha_{\text{i2t}} - s(v,t) + s(v,t^-)]_+ \\ &+ [\alpha_{\text{t2i}} - s(v,t) + s(v^-,t)]_+.\end{aligned} \tag{5}$$

The descriptiveness scores in the adaptive margin control the discrimination between positive and negative pairs. More concretely, sentences providing general explanation are more likely to be positives, suggesting that the margin should be relaxed accordingly. Thus, the separation constraint is decreased for pairs with general descriptions (*i.e.*, low $\delta(\cdot)$), such that their shared semantics are preserved across other specific sentences and images. In contrast, for highly descriptive sentences in both positive and negative pairs, the model enforces

TABLE I: Experimental results on MS-COCO [8] 1K and 5K Test Images. * used additional augmentation strategies.

Backbone	Method	1K Test Images							5K Test Images						
		Image-to-Text			Text-to-Image			RSUM	Image-to-Text			Text-to-Image			RSUM
		R@1	R@5	R@10	R@1	R@5	R@10		R@1	R@5	R@10	R@1	R@5	R@10	
ViT-B/32 (151M)	CLIP ZS [48]	69.1	90.9	95.7	49.7	79.3	88.8	473.6	50.0	74.9	83.5	30.5	56.0	66.9	361.7
	DAA [3]	74.4	95.3	98.3	65.0	91.3	96.5	520.9	52.7	80.1	88.8	43.3	72.4	82.6	419.9
	InfoNCE [2]	77.3	95.7	98.4	64.2	91.1	96.5	523.3	55.3	82.7	90.6	41.6	72.1	82.7	425.1
	PCME [16]	80.1	96.3	98.7	67.4	92.2	97.0	531.6	59.8	85.3	92.0	45.9	75.0	84.5	442.5
	SAM [4]	81.4	96.7	98.9	68.0	92.5	97.0	534.5	61.5	86.3	92.7	46.8	75.6	84.9	447.8
	PCME++* [13]	81.8	97.1	98.9	69.0	92.7	96.9	536.6	61.9	87.1	93.3	48.1	76.6	85.6	452.7
	VSE++ [1]	82.1	96.9	99.1	69.2	92.7	96.8	536.8	63.3	87.1	92.7	48.3	76.6	85.5	453.5
	DITM	**83.7**	**97.4**	**99.2**	**70.1**	**92.8**	**97.1**	**540.3**	**65.0**	**88.4**	**94.1**	**49.3**	**77.3**	**86.0**	**460.3**
ViT-B/16 (150M)	CLIP ZS [48]	71.7	91.6	96.5	52.4	80.9	89.8	482.8	52.5	76.7	84.6	33.1	58.4	69.0	374.4
	DAA [3]	79.0	96.4	98.8	69.6	93.3	97.5	534.6	59.6	85.1	92.3	48.5	77.2	86.0	448.6
	InfoNCE [2]	81.6	97.3	99.1	69.6	93.1	97.2	538.0	62.2	87.2	93.7	47.8	77.0	86.0	454.0
	PCME [16]	83.4	97.6	99.3	71.6	93.7	97.6	543.2	65.0	89.2	94.5	50.9	78.9	87.3	465.7
	SAM [4]	84.1	97.6	99.2	72.5	94.1	97.7	545.3	66.9	89.1	94.3	52.3	79.7	87.8	470.0
	VSE++ [1]	85.2	97.8	99.3	73.5	94.2	97.5	547.5	68.3	89.8	94.5	53.6	80.2	88.0	474.4
	PCME++* [13]	85.2	98.0	**99.5**	73.4	**94.4**	**97.9**	548.4	68.5	89.9	95.2	53.5	80.3	88.4	475.8
	DITM	**86.4**	**98.1**	99.4	**74.5**	94.3	97.8	**550.5**	**70.4**	**90.8**	**95.3**	**54.7**	**81.3**	**88.9**	**481.4**
ViT-L/14 (428M)	CLIP ZS [48]	74.2	92.9	97.1	55.4	82.3	91.0	493.0	56.3	79.4	86.6	36.5	61.0	71.1	391.0
	InfoNCE [2]	81.4	97.4	99.3	68.9	93.2	97.2	537.3	60.2	87.5	93.5	47.2	77.1	86.1	451.7
	PCME [16]	86.0	97.9	99.5	74.3	94.7	97.7	550.0	69.9	90.6	95.4	54.4	81.3	89.1	480.6
	VSE++ [1]	86.2	98.2	99.5	75.3	94.5	97.6	551.3	70.6	91.0	95.7	56.5	82.2	89.4	485.5
	PCME++* [13]	87.2	98.2	99.3	75.8	**95.2**	**98.1**	553.9	71.1	92.1	96.2	56.7	82.9	**90.1**	489.1
	DITM	**87.6**	**98.5**	**99.5**	**76.3**	95.1	98.0	**554.8**	**72.0**	**92.6**	**96.4**	**57.3**	**83.0**	90.0	**491.3**

a stricter separation to ensure a clear distinction between irrelevant pairs. Such flexibility of our adaptive triplet loss prevents the model from improperly separating semantically relevant pairs while effectively distinguishing true negatives.

D. Learning generic-to-specific order of multiple texts

While the adaptive triplet loss captures relationships between positive and negative samples, the embedding space remains insufficient for representing the graded contextual similarities between an image and its relevant sentences. To address this, we employ a hierarchical structure that enables the model to learn cross-modal representations at different levels of abstraction, reflecting how humans perceive and understand information. Specifically, for a given image with multiple descriptions, a sentence with more instance-specific information is contextually closer to the image than one with less detail. To this end, we propose a generic-to-specific ordering loss that approximates the ratio of pairwise image-sentence distances as the inverse ratio of their corresponding sentence descriptiveness scores. Our generic-to-specific ordering loss is inspired by [35], which approximates the image distances as their label distances, but we extend this idea into a form suitable for learning cross-modal relationships between an image and its relevant sentences.

Given a triplet of an image v and its two positive sentences t, t^+, the objective is defined as:

$$\mathcal{L}_{\text{Order}} = \sum_{(v,t,t^+)} \left\{ \log \frac{d(v,t)}{d(v,t^+)} - \log \frac{\delta(t^+)}{\delta(t)} \right\}^2, \qquad (6)$$

where $d(\cdot,\cdot)$ represents the Euclidean distance between L2-normalized cross-modal embedding vectors. The loss enforces the most descriptive sentence to be the closest to its paired image. Ideally, a sentence with the highest descriptiveness will be the closest to an image, and the distance will gradually increase as the descriptiveness gets smaller. This property of the objective enhances the fine-grained distinctions between several sentences and allows the model to capture the many-to-many nature of vision and language.

We train DITM using the proposed adaptive triplet loss and generic-to-specific ordering loss simultaneously, as follows:

$$\mathcal{L}_{\text{Overall}} = \mathcal{L}_{\text{AdaTrp}} + \lambda \mathcal{L}_{\text{Order}}, \qquad (7)$$

where λ is a balancing parameter.

IV. Experiments

A. Datasets

We evaluate our DITM on four ITM benchmarks: MS-COCO [8], Flickr30K [9], Crisscrossed Captions (CxC) [23] and HierarCaps [24]. The MS-COCO consists of 123,287 images, where 113,287/5,000/5,000 images are used for train/validation/test sets [47]. We evaluate our method on both 1K and 5K test images, in which the 1K results are an average over 5-fold test split. For the Flickr30K of a total of 31,000 images, we leverage 29,000/1,000/1,000 images for each train/validation/test set [1]. Both the MS-COCO and Flickr30K provide five corresponding sentences per image. The CxC extends the sparse annotations of the MS-COCO test set by incorporating additional human semantic similarity judgments on both inter-modal and intra-modal pairs. The HierarCaps augments the MS-COCO validation set by constructing four-level sentence hierarchies through the LLM Llama 2 [49] along with heavy natural language inference filtering (*e.g.*, "food" ⇒ "hot dog" ⇒ "hot dog on plate" ⇒ "a hot dog on a plate next to two glasses"). For each dataset, we pre-compute the

TABLE II: Experimental results on Flickr30K [9] and CxC [23] datasets. * used additional augmentation strategies.

Method	Flickr30K							CxC							
	I→T			T→I			RSUM	I→T		T→I		I→I		T→T	
	R@1	R@5	R@10	R@1	R@5	R@10		R@1	R@5	R@1	R@5	R@1	R@5	R@1	R@5
CLIP ZS [48]	78.8	94.9	98.2	58.8	83.5	90.0	504.3	51.6	77.3	32.3	58.8	31.5	62.5	35.2	55.5
InfoNCE [2]	67.0	87.5	93.0	51.8	80.9	88.5	468.7	57.0	84.4	43.7	74.5	44.5	77.9	43.3	65.9
PCME [16]	71.3	92.1	96.5	59.0	85.8	91.5	496.1	61.2	87.0	47.9	77.1	45.1	**79.5**	44.6	67.5
DAA [3]	82.7	96.6	98.6	68.2	90.5	94.9	531.5	54.6	82.3	45.3	74.6	**45.8**	79.2	43.0	65.8
PCME++* [13]	83.8	96.5	98.9	70.0	91.3	95.2	535.7	63.5	88.6	50.0	78.7	44.7	78.7	44.9	67.8
SAM [4]	86.9	98.0	**99.6**	72.4	92.6	96.1	545.7	63.0	88.0	48.8	77.8	45.5	79.4	45.1	68.1
VSE++ [1]	87.6	97.9	99.1	71.9	91.9	95.8	544.2	64.8	88.8	50.4	78.5	45.5	79.0	45.2	**68.5**
DITM	**88.4**	**98.3**	**99.6**	**73.6**	**92.7**	**96.2**	**548.7**	**66.2**	**89.6**	**51.2**	**79.3**	45.5	78.8	**45.3**	68.3

TABLE III: Experimental results on the HierarCaps [24] dataset. * used additional augmentation strategies.

Method	P	R	d_{corr}
CLIP ZS [48]	28.0	22.1	75.8
InfoNCE [2]	20.0	24.9	67.0
VSE++ [1]	22.2	23.6	76.0
PCME [16]	23.3	23.2	70.0
PCME++* [13]	25.0	21.0	73.1
DAA [3]	28.0	16.7	66.1
SAM [4]	**33.2**	17.8	72.4
DITM	28.7	**26.2**	**83.3**

descriptiveness score for each sentence, using the sentences from the train set as the document pool $\mathcal{T}$.

B. Evaluation metrics

The standard evaluation metric for ITM is recall at K (R@K), indicating the presence of query-relevant items in the top-K retrieved results. For the MS-COCO and Flickr30K, we report results for $K = \{1, 5, 10\}$, along with their summation, *i.e.*, RSUM. For the CxC, we report results for $K = \{1, 5\}$ across four retrieval directions. To evaluate hierarchical ITM on the HierarCaps, we perform retrieval by traversing from the closest text embedding of a given image to the root node (the null text embedding " "). Following previous works [24], [50], [51], we interpolate between the text embedding and the root node with 50 equally spaced points, and retrieve the closest text embedding at each point. Given the set of retrieved texts, we compute precision and recall, which measure how many of the retrieved texts are correct and how many of the correct texts the model managed to retrieve. In addition, we report order-aware metric d_{corr} to check whether the four ground truth hierarchy sentences are correctly ordered by their distances from the corresponding image. While [24] computes d_{corr} by distances from the root node, we substitute it with the image to better evaluate the relationships between images and texts.

C. Implementation details

1) Network architecture: While DITM can be applied to existing ITM approaches, we focus on dual-encoder architectures [48], [52] for computational efficiency. Following [13], we adopt a generalized pooling operator (GPO) [52] atop a Vision Transformer (ViT) [53] to make an image encoder. We use a 12-layer 512-wide Transformer [54] as our text encoder. The extracted feature representations are l2-normalized.

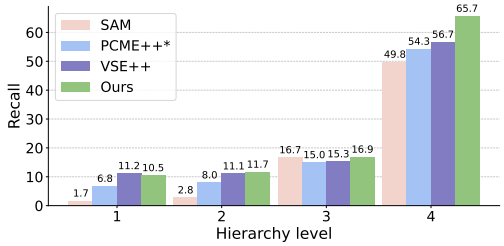

Fig. 5: Per-level recall analysis on the HierarCaps [24] dataset. * used additional augmentation strategies.

2) Training settings: We initialize the backbone networks with the pre-trained CLIP model [48] and randomly initialize the GPO. We train all models with batch size 128 for 25 epochs using AdamP optimizer [55] with initial learning rate of 5e-4 and a weight decay of 1e-4. The learning rate is decayed by $0.1\times$ after 15 epochs. Following [13], [52], we use learning rate multipliers: $0.01\times$ for visual and $0.1\times$ for textual backbones. As a warm-up strategy, we freeze the visual backbone and include the hardest negative mining except for the first two epochs. For each transformer block, layer-wise learning rate decay is applied by 0.7. The scaling factor for our adaptive margin and balancing parameter for the total loss functions are set to $\tau = 6$ and $\lambda = 0.07$, respectively.

D. Quantitative results

1) Comparison methods: We present the performance comparisons with the previous ITM objectives, including one-to-one pairwise learning objectives [1], [2], dense labeling approaches [3], [4], and probabilistic approaches [13], [16].

- **One-to-one pairwise learning.** VSE++ [1] is the standard ITM objective where the hardest negative mining strategy is incorporated into a triplet loss as described in Eq. 3. InfoNCE [2] is the pre-training objective for CLIP [48], which maximizes the mutual information between the positive pairs. The objectives solely rely on sparse binary supervision of ITM benchmarks and focus on enlarging the similarities of positive pairs while reducing the similarities of negative pairs.
- **Dense labeling approaches.** SAM [4] and DAA [3] densely define the relevance score for every image-text pair. To measure the relevance between an image and the unpaired text sample, they leverage five positive texts associated with the given image and measure the similarity between these five texts and the text being evaluated,

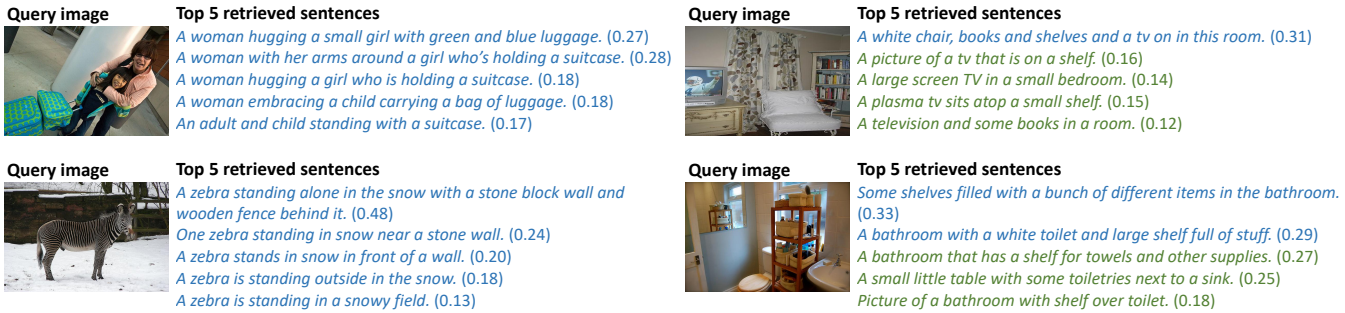

(a) Image-to-text retrieval results

(b) Text-to-image retrieval results

Fig. 6: Qualitative results of image-text retrieval on the MS-COCO [8] dataset. True positives, false negatives, and true negatives are marked in blue, green, and red, respectively. The descriptiveness scores are rounded to two decimal places for clear illustration. For text-to-image retrieval, the two query sentences in each row are paired with the same image.

using CIDEr metric [15]. DAA additionally incorporates the image-text similarity score predicted by the model, and proposes a differentiable ranking-based objective. Similar to our method, SAM introduces an adaptive margin into the triplet loss based on the relevance score. Both SAM and DAA act as an additional regularization term on top of the hinge-based triplet ranking loss.

- **Probabilistic approaches.** PCME [16] is a pioneering work for probabilistic ITM with sampling-based matching probability. PCME++ [13] extends PCME by removing the sampling procedure through closed sample distance between the probability distributions. To improve the overall accuracy, PCME++ adopts additional mixed sample data augmentation strategies (*i.e.*, input mixing and label mixing [56], [57]). These strategies are hard to apply in other batch-dependent objectives [1]–[4], including our DITM, since a mixed sample influences the other samples in the batch as well.

All methods are implemented on the same visual and textual backbones as our model, except the probabilistic approaches that require an additional prediction head for the variance vector. Since they are built on the pre-trained CLIP model, we also report its zero-shot performance, CLIP ZS, as a baseline.

2) MS-COCO: In Tab. I, we compare our results to the SOTA ITM objectives on the MS-COCO [8] dataset. We train the models with three variants of ViT, including ViT-B/32, ViT-B/16, and ViT-L/14. Our DITM establishes new SOTA performances across most recall metrics, demonstrating the effectiveness of exploring the descriptive level of each sentence for ITM. Specifically, ours with ViT-B/32 backbone achieves 3.5%p and 6.8%p performance improvements over VSE++ in terms of RSUM on each 1K and 5K test images. While the improvements with ViT-L/14 are smaller, the consistent gains across diverse backbone sizes demonstrate the scalability and robustness of our method across varying model capacities.

3) Flickr30K: We evaluate the performance on the Flickr30K [9] dataset in Tab. II. We restrict our experiments to models with ViT-B/32 backbone, considering the smaller scale of the dataset. While our adaptive margin shares a similar formulation with the SAM approach, they mainly differ in how the relevance of each image-sentence pair is defined. Specifically, the text similarities employed in SAM cannot fully capture how a text matches the visual content of an image—some visual aspects may be omitted or underemphasized in the text descriptions. To mitigate the problem of improper correspondences, we alleviate the given binary label of ITM benchmarks based on the descriptiveness of each

TABLE IV: Ablation study for the impact of each loss in our DITM on the MS-COCO [8], Flickr30K [9], CxC [23], and HierarCaps [24] datasets.

	Method	MS-COCO 1K R@1	MS-COCO 1K RSUM	MS-COCO 5K R@1	MS-COCO 5K RSUM	Flickr30K R@1	Flickr30K RSUM	CxC R@1	CxC RSUM	HierarCaps P	HierarCaps R	HierarCaps d_{corr}
(i)	Conventional triplet loss	75.7	536.8	55.8	453.5	79.8	544.2	51.5	520.7	22.2	23.6	76.0
(ii)	Adaptive triplet loss	76.0	539.0	56.4	457.1	80.0	544.8	**52.1**	522.3	24.6	25.6	76.6
(iii)	(ii) + Generic-to-specific ordering loss	**76.9**	**540.3**	**57.2**	**460.3**	**80.8**	**548.7**	**52.1**	**524.2**	**28.7**	**26.2**	**83.3**

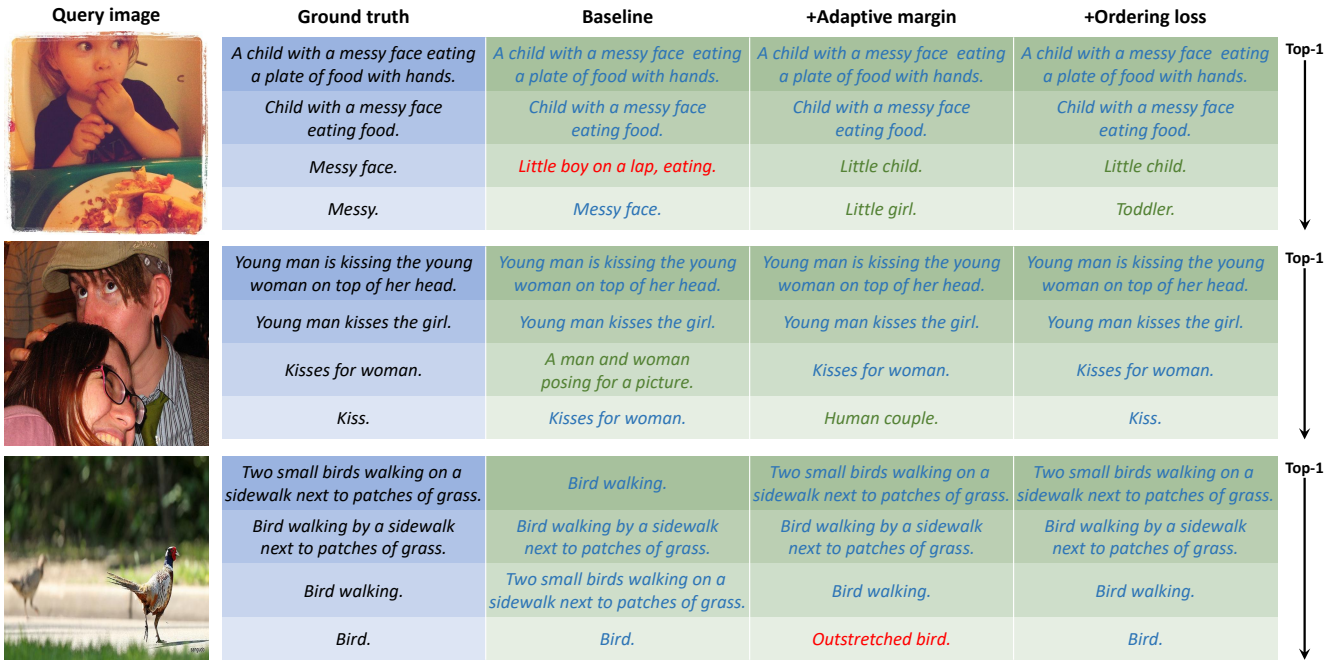

Fig. 7: Qualitative results of image-to-text retrieval on the HierarCaps [24] dataset. We mark the true positive, false negative, and true negative sentences in blue, green, and red, respectively.

sentence, outperforming SAM by 3.0%p in terms of RSUM.

4) Crisscrossed Captions (CxC): In Tab. II, we provide the results evaluated on the Crisscrossed Captions (CxC) [23] dataset. The increased density of their annotations more effectively evaluates the model capacity to represent the many-to-many relationships between vision and language. Our method outperforms SOTAs in inter-modal retrieval, achieving 1.4% and 0.8% performance improvements over VSE++ in terms of R@1 on image-to-text and text-to-image retrieval, respectively. Our DITM also shows competitive performances on intra-modal retrievals, while a slight trade-off in image-to-image retrieval suggests that narrowing the cross-modal gap may influence intra-modal relationship. As discussed in [58], this trade-off can be effectively mitigated through additional intra-modal similarity learning losses.

5) HierarCaps: Tab. III shows the results on the HierarCaps [24] dataset for hierarchical ITM. We achieve the best performances with recall of 26.2% and d_{corr} of 83.3%. While SAM attains the highest precision, its notably low recall indicates that the model is overly selective and fails to retrieve many of the true sentences. In contrast, our method maintains competitive precision and a much higher recall.

For in-depth analysis, we also compare per-level recall of SAM, PCME++, VSE++, and our DITM. As shown in Fig. 5, SAM excels in retrieving third- and fourth-level sentences but struggles with first- and second-level ones. This indicates that SAM performs well only on sentences with a descriptive level similar to the ones in training data; sentences in MS-COCO mostly correspond to the fourth-level. Meanwhile, our method shows more balanced results across all descriptive levels, highlighting its effectiveness in representing the sentence hierarchies. Overall, our DITM not only provides robust retrieval coverage and accurate ordering of sentence hierarchies but also maintains a favorable trade-off between precision and recall.

E. Qualitative results

In Fig. 6, we provide qualitative results of image-text retrieval on the MS-COCO dataset. Given a query, we depict the top-5 retrieved items and the sentence descriptiveness scores, computed using the sentences from test set as the document pool. Note that the descriptiveness score on the test sample is measured for explanation only, not used during prediction. In image-to-text retrieval, some of the retrieved sentences are labeled as negatives but are all in fact the truthful sentences (*i.e.*, false negatives). Notably, the rank of the retrieved sentences follows a generic-to-specific order; the most specific descriptions (*i.e.*, including descriptions for specific colors, objects, etc) ranked as the first, and the most general descriptions ranked as the last. In text-to-image retrieval in Fig. 6-(b), we present different retrieval results for two semantically relevant sentences (per row). While general descriptions can be mapped to a lot of diverse images, the exact annotations for the

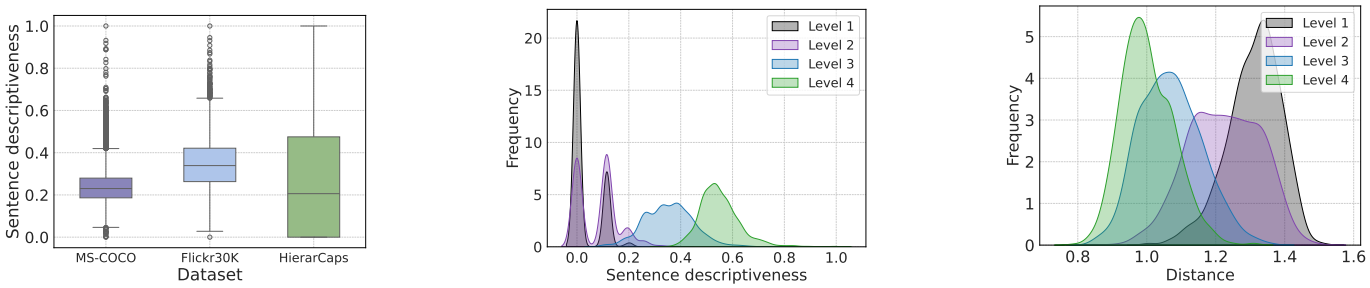

(a) Dataset statistics (b) Descriptiveness statistics (c) Distance statistics

Fig. 8: (a) Distributions of sentence descriptiveness in the MS-COCO [8], Flickr30K [9], and HierarCaps [24] test sets. (b) Distributions of sentence descriptiveness scores for each hierarchy level in the HierarCaps dataset. (c) Distributions of image-sentence distances for each hierarchy level in the HierarCaps.

TABLE V: Ablation study for the scaling factor τ on the MS-COCO [8], Flickr30K [9], and CxC [23] datasets.

Dataset	τ ($\lambda = 0.07$)			λ ($\tau = 6$)			
	5	6	7	0.06	0.07	0.08	0.09
COCO 1K	538.5	**540.3**	538.5	539.8	**540.3**	539.1	538.7
COCO 5K	458.3	**460.3**	458.5	459.4	**460.3**	458.8	457.3
Flickr30K	545.0	**548.7**	544.2	546.2	**548.7**	547.6	546.6
CxC	523.3	**524.2**	522.4	524.1	**524.2**	522.7	521.8

possible matches are omitted in ITM benchmarks. However, our method manages to retrieve truthful images (samples on left). As the sentence becomes more specific (samples on right), the diversity of the truthful images narrows down to the ground-truth image. By learning fine-grained image-text alignments through the graded contextual similarity, our DITM correctly retrieves the ground truth images corresponding to the instance-specific information described in the sentence.

F. Ablation study

1) Component analysis: We analyze the impact of the adaptive margin in $\mathcal{L}_{\text{AdaTrp}}$ and the generic-to-specific ordering loss $\mathcal{L}_{\text{Order}}$. For clear illustration, we report the average R@1 over all retrieval directions and RSUM on the MS-COCO, Flickr30K, and CxC. Since $\mathcal{L}_{\text{AdaTrp}}$ incorporates an adaptive margin into the triplet ranking loss with online hard negative mining, we measure the performance improvements over the VSE++ [1] baseline. As shown in Tab. IV, the inclusion of adaptive margin introduces considerable gains in most metrics, achieving 2.2%p and 3.6%p improvements in terms of RSUM on MS-COCO 1K and 5K, respectively. This demonstrates that the alleviated relationships using the sentence descriptiveness effectively preserves the shared semantics of possible positives, thereby improving the overall performance. Meanwhile, the inclusion of ordering loss $\mathcal{L}_{\text{Order}}$ further attains 0.7%p and 3.2%p performance improvements in terms of RSUM on each MS-COCO 1K and 5K. In addition, the ordering objective introduces a larger boost in order-aware metric, yielding 6.6% performance improvements in terms of d_{corr}. These observations indicate that differentiating the contextual similarity based on the descriptive level of sentences enhances the hierarchical understanding of the model and enables stronger alignment between images and texts.

To better understand the impact of each component, we also visualize the image-text retrieval results on the HierarCaps dataset in Fig. 7. Although all three methods generally retrieve query-relevant sentences, the baseline often presents results in a less organized manner. By incorporating our adaptive margin, the retrieved sentences are ordered in a generic-to-specific order, and the inclusion of the ordering loss further enables the model to understand the sentence hierarchies.

2) Visualization of sentence descriptiveness: To validate the effectiveness of our formulation for the sentence descriptiveness score, we visualize their statistics. In Fig. 8-(a), we depict the distribution of descriptiveness scores in the MS-COCO, Flickr30K, and HierarCaps test sets (the CxC is omitted since it uses the same sentences as the MS-COCO). The scores of the MS-COCO and Flickr30K have narrower spreads, which indicates that most of their sentences have similar descriptive level. In contrast, the HierarCaps exhibits a wider range since it contains four distinct descriptive levels.

To analyze the statistics of the HierarCaps in detail, we separately visualize the distribution of the sentence descriptiveness across four hierarchy levels in Fig. 8-(b). Since the levels 1 and 2 typically contain one-word sentences, their descriptiveness values are located near zero. Meanwhile, the levels 3 and 4, where the sentences are longer and more specific, tend to have progressively higher ranges, confirming that our sentence descriptiveness effectively reflects the graded contextual similarity between images and texts. We also depict how the distances between sentences and the corresponding images shift by level in Fig. 8-(c). The sentences of level 1 demonstrate the largest distances, while the sentences of level 4 exhibits the smallest. The result coincides with the intent of our proposed ordering objective, which enforces the most descriptive sentence to be the closest to its corresponding image. Taken together, these distributions underscore the effectiveness of our method in learning image-text relationships by exploring the descriptive level of the sentences.

3) Effect of scaling factor: The scaling factor τ controls the width of our adaptive margin in Eq. 4. To study its effect, we compare the performance in terms of RSUM across different values of τ on the MS-COCO, Flickr30K, and CxC. As shown in Tab. V, overall tendency across three datasets is similar where the optimal result are obtained with $\tau = 6$ While our method requires careful tuning of τ, the gains over the fixed

margin confirms the importance of our adaptive margin in learning complex image-text relationships.

4) Effect of balancing parameter: The balancing parameter λ controls the impact of generic-to-specific ordering loss $\mathcal{L}_{\text{Order}}$ in the total objective. To examine its sensitivity, we report the performance in terms of RSUM according to λ in Tab. V. The inclusion of $\mathcal{L}_{\text{Order}}$ introduces consistent gain, where the best performance is attained with $\lambda = 0.07$ on all three datasets, validating its effectiveness in improving the fine-grained distinctions between image and text representations.

V. Conclusion

In this paper, we have introduced novel image-text matching objectives, DITM, using the descriptive flexibility of language. Our approach learns broader image-text relationships by alleviating given image-text correspondences in existing ITM benchmarks. We have efficiently formulated descriptiveness scores of sentences based on word statistics from the training set. The sentence descriptiveness has been incorporated into our adaptive triplet loss as adaptive margins, and generic-to-specific ordering loss. Our proposed triplet loss relaxes the false negative penalty while ensuring strict separation of irrelevant pairs. Our ordering loss improves graded alignment of image-text pairs by weighting generic-to-specific order. Extensive experiments have demonstrated the effectiveness of our DITM in learning complex image-text relationships.

References

[1] F. Faghri, D. J. Fleet, J. R. Kiros, and S. Fidler, "Vse++: Improving visual-semantic embeddings with hard negatives," *BMVC*, 2017.

[2] Y. Zhang, H. Jiang, Y. Miura, C. D. Manning, and C. P. Langlotz, "Contrastive learning of medical visual representations from paired images and text," *arXiv preprint arXiv:2010.00747*, 2020.

[3] H. Li, J. Song, L. Gao, P. Zeng, H. Zhang, and G. Li, "A differentiable semantic metric approximation in probabilistic embedding for cross-modal retrieval," *NeurIPS*, 2022.

[4] A. F. Biten, A. Mafla, L. Gómez, and D. Karatzas, "Is an image worth five sentences? a new look into semantics for image-text matching," *WACV*, 2022.

[5] A. Frome, G. Corrado, J. Shlens, S. Bengio, J. Dean, M. Ranzato, and T. Mikolov, "Devise: A deep visual-semantic embedding model," *NeurIPS*, 2013.

[6] J. Wei, X. Xu, Y. Yang, Y. Ji, Z. Wang, and H. T. Shen, "Universal weighting metric learning for cross-modal matching," *CVPR*, 2020.

[7] S. Chun, W. Kim, S. Park, M. Chang, and S. J. Oh, "Eccv caption: Correcting false negatives by collecting machine-and-human-verified image-caption associations for ms-coco," *ECCV*, 2022.

[8] X. Chen, H. Fang, T.-Y. Lin, R. Vedantam, S. Gupta, P. Dollár, and C. L. Zitnick, "Microsoft coco captions: Data collection and evaluation server," *arXiv preprint arXiv:1504.00325*, 2015.

[9] P. Young, A. Lai, M. Hodosh, and J. Hockenmaier, "From image descriptions to visual denotations: New similarity metrics for semantic inference over event descriptions," *TACL*, vol. 2, 2014.

[10] R. Kiros, R. Salakhutdinov, and R. S. Zemel, "Unifying visual-semantic embeddings with multimodal neural language models," *NeurIPS*, 2014.

[11] L. Wang, Y. Li, and S. Lazebnik, "Learning deep structure-preserving image-text embeddings," *CVPR*, 2016.

[12] T. Chen, J. Deng, and J. Luo, "Adaptive offline quintuplet loss for image-text matching," *ECCV*, 2020.

[13] S. Chun, "Improved probabilistic image-text representations," *ICLR*, 2024.

[14] M. Zhou, Z. Niu, L. Wang, Z. Gao, Q. Zhang, and G. Hua, "Ladder loss for coherent visual-semantic embedding," *AAAI*, 2020.

[15] R. Vedantam, C. Lawrence Zitnick, and D. Parikh, "Cider: Consensus-based image description evaluation," *CVPR*, 2015.

[16] S. Chun, S. J. Oh, R. S. de Rezende, Y. Kalantidis, and D. Larlus, "Probabilistic embeddings for cross-modal retrieval," *CVPR*, 2021.

[17] L. Zhang, D. Zhou, Y. He, and Z. Yang, "Merl: Multimodal event representation learning in heterogeneous embedding spaces," *AAAI*, 2021.

[18] U. Upadhyay, S. Karthik, M. Mancini, and Z. Akata, "Probvlm: Probabilistic adapter for frozen vison-language models," *ICCV*, 2023.

[19] Y. Song and M. Soleymani, "Polysemous visual-semantic embedding for cross-modal retrieval," *CVPR*, 2019.

[20] D. Kim, N. Kim, and S. Kwak, "Improving cross-modal retrieval with set of diverse embeddings," *CVPR*, 2023.

[21] G. Salton and C. Buckley, "Term-weighting approaches in automatic text retrieval," *Information processing & management*, vol. 24, 1988.

[22] A. Aizawa, "An information-theoretic perspective of tf–idf measures," *Information Processing & Management*, vol. 39, 2003.

[23] Z. Parekh, J. Baldridge, D. Cer, A. Waters, and Y. Yang, "Crisscrossed captions: Extended intramodal and intermodal semantic similarity judgments for ms-coco," *EACL*, 2021.

[24] M. Alper and H. Averbuch-Elor, "Emergent visual-semantic hierarchies in image-text representations," *ECCV*, 2024.

[25] K.-H. Lee, X. Chen, G. Hua, H. Hu, and X. He, "Stacked cross attention for image-text matching," *ECCV*, 2018.

[26] Q. Zhang, Z. Lei, Z. Zhang, and S. Z. Li, "Context-aware attention network for image-text retrieval," *CVPR*, 2020.

[27] K. Zhang, Z. Mao, Q. Wang, and Y. Zhang, "Negative-aware attention framework for image-text matching," *CVPR*, 2022.

[28] S. Pang, Y. Zeng, J. Zhao, and J. Xue, "A mutually textual and visual refinement network for image-text matching," *TMM*, 2024.

[29] D. Wu, H. Li, C. Gu, L. Guo, and H. Liu, "Dual stream relation learning network for image-text retrieval," *TMM*, 2024.

[30] F. Locatello, D. Weissenborn, T. Unterthiner, A. Mahendran, G. Heigold, J. Uszkoreit, A. Dosovitskiy, and T. Kipf, "Object-centric learning with slot attention," *NeurIPS*, vol. 33, 2020.

[31] Z. Wang, Z. Gao, X. Xu, Y. Luo, Y. Yang, and H. T. Shen, "Point to rectangle matching for image text retrieval," *ACMMM*, 2022.

[32] Z. Wang, Z. Gao, M. Han, Y. Yang, and H. T. Shen, "Estimating the semantics via sector embedding for image-text retrieval," *TMM*, 2024.

[33] P. Hu, X. Peng, H. Zhu, L. Zhen, and J. Lin, "Learning cross-modal retrieval with noisy labels," *CVPR*, 2021.

[34] Z. Huang, G. Niu, X. Liu, W. Ding, X. Xiao, H. Wu, and X. Peng, "Learning with noisy correspondence for cross-modal matching," *NeurIPS*, vol. 34, 2021.

[35] S. Kim, M. Seo, I. Laptev, M. Cho, and S. Kwak, "Deep metric learning beyond binary supervision," *CVPR*, 2019.

[36] S. Yang, W. Yu, Y. Zheng, H. Yao, and T. Mei, "Adaptive semantic-visual tree for hierarchical embeddings," *ACMMM*, 2019.

[37] T. Chen, W. Wu, Y. Gao, L. Dong, X. Luo, and L. Lin, "Fine-grained representation learning and recognition by exploiting hierarchical semantic embedding," *ACMMM*, 2018.

[38] B. Barz and J. Denzler, "Hierarchy-based image embeddings for semantic image retrieval," *WACV*, 2019.

[39] C.-A. Brust and J. Denzler, "Integrating domain knowledge: using hierarchies to improve deep classifiers," *ACPR*, 2019.

[40] A. Lai and J. Hockenmaier, "Illinois-lh: A denotational and distributional approach to semantics." *SemEval*, 2014.

[41] D. Han, P. Martínez-Gómez, and K. Mineshima, "Visual denotations for recognizing textual entailment," *EMNLP*, 2017.

[42] A. Lai and J. Hockenmaier, "Learning to predict denotational probabilities for modeling entailment," *EACL*, 2017.

[43] B. Zhang, H. Hu, V. Jain, E. Ie, and F. Sha, "Learning to represent image and text with denotation graph," *EMNLP*, 2020.

[44] S. Changpinyo, P. Sharma, N. Ding, and R. Soricut, "Conceptual 12m: Pushing web-scale image-text pre-training to recognize long-tail visual concepts," *CVPR*, 2021.

[45] C. Schuhmann, R. Beaumont, R. Vencu, C. Gordon, R. Wightman, M. Cherti, T. Coombes, A. Katta, C. Mullis, M. Wortsman *et al.*, "Laion-5b: An open large-scale dataset for training next generation image-text models," *NeurIPS*, vol. 35, 2022.

[46] B. Zhang, H. Hu, L. Qiu, P. Shaw, and F. Sha, "Visually grounded concept composition," *EMNLP*, 2021.

[47] A. Karpathy and L. Fei-Fei, "Deep visual-semantic alignments for generating image descriptions," *CVPR*, 2015.

[48] A. Radford, J. W. Kim, C. Hallacy, A. Ramesh, G. Goh, S. Agarwal, G. Sastry, A. Askell, P. Mishkin, J. Clark *et al.*, "Learning transferable visual models from natural language supervision," *ICML*, 2021.

[49] H. Touvron, L. Martin, K. Stone, P. Albert, A. Almahairi, Y. Babaei, N. Bashlykov, S. Batra, P. Bhargava, S. Bhosale *et al.*, "Llama 2: Open foundation and fine-tuned chat models," *arXiv preprint arXiv:2307.09288*, 2023.

[50] K. Desai, M. Nickel, T. Rajpurohit, J. Johnson, and S. R. Vedantam, "Hyperbolic image-text representations," *ICML*, 2023.
[51] S. Chun, W. Kim, S. Park, and S. Yun, "Probabilistic language-image pre-training," *arXiv preprint arXiv:2410.18857*, 2024.
[52] J. Chen, H. Hu, H. Wu, Y. Jiang, and C. Wang, "Learning the best pooling strategy for visual semantic embedding," *CVPR*, 2021.
[53] A. Dosovitskiy, "An image is worth 16x16 words: Transformers for image recognition at scale," *ICLR*, 2021.
[54] A. Vaswani, N. Shazeer, N. Parmar, J. Uszkoreit, L. Jones, A. N. Gomez, Ł. Kaiser, and I. Polosukhin, "Attention is all you need," *NeurIPS*, 2017.
[55] B. Heo, S. Chun, S. J. Oh, D. Han, S. Yun, G. Kim, Y. Uh, and J.-W. Ha, "Adamp: Slowing down the slowdown for momentum optimizers on scale-invariant weights," *ICLR*, 2021.
[56] H. Zhang, M. Cisse, Y. N. Dauphin, and D. Lopez-Paz, "mixup: Beyond empirical risk minimization," *arXiv preprint arXiv:1710.09412*, 2017.
[57] S. Yun, D. Han, S. J. Oh, S. Chun, J. Choe, and Y. Yoo, "Cutmix: Regularization strategy to train strong classifiers with localizable features," *ICCV*, 2019.
[58] M. Mistretta, A. Baldrati, L. Agnolucci, M. Bertini, and A. D. Bagdanov, "Cross the gap: Exposing the intra-modal misalignment in clip via modality inversion," *ICLR*, 2025.